RSC Advances

ROYAL SOCIETY OF CHEMISTRY

www.rsc.org/advances

Fully screen printed highly conductive electrodes on various flexible substrates for asymmetric supercapacitors

Siliang Wang,[a] Nishuang Liu,*[a] Congxing Yang,[a] Weijie Liu,[a] Jun Su,[a] Luying Li,[a] Changping Yang[b] and Yihua Gao*[ab]

Highly flexible conductive electrodes have been successfully prepared by screen printing commercial carbon nanoparticle ink onto various substrates, such as clothes, polyethylene terephthalate (PET) and paper. The flexible electrodes showed good stability during the bending test and could act as a foldable electric circuit. Step more, multi-walled carbon nanotubes-manganese dioxide (MWCNTs-MnO_2) anode and multi-walled carbon nanotubes-molybdenum trioxide (MWCNTs-MoO_3) cathode for asymmetric supercapacitors (ASCs) were screen printed onto carbon nanoparticle electrodes that acted as collector. The fully screen printed supercapacitor has a wide operating potential window of 1.7 V and exhibits excellent electrochemical performance, *e.g.* a high energy density of 11.04 mWh cm^{-3} at a power density of 614.6 mW cm^{-3}, a high retained ratio ~91.3% of its initial capacitance after 5000 cycles. The screen-printing acting as a simple, versatile, fast, cost-effective printing techniques method can be fully integrated with the fabrication process in current printed electronics and has potential applications for energy storage.

Introduction

Flexible displays,[1, 2] flexible and conformal antenna arrays,[3, 4] electric circuits and chemical sensor,[5] electronic solar cell arrays,[6] radio frequency identification tags,[7] microstructure electrochemical capacitors[8-10] as flexible optoelectronic and electronic devices have gained rapid developments and promoted the demands for high-performance flexible conductive electrodes.

There are many ways to produced flexible conductive electrodes such as sputtering,[11, 12] chemical vapor deposition[13] and Filtrating.[14] These methods are widely thought to be a high-cost process, for the use of large scale equipment with a vacuum system and the complicated steps in the process. Screen printing is one of most simple, versatile, fast and cost-effective printing techniques to make flexible conductive electrodes. It does not require expensive vacuum technology and can be applied to any surface shape and size, such as glass, plastics, or clothes. Future developments are aiming at light, thin, cheap, flexible and sustainable solutions, with wearable electronics as one typical application. More specifically, "printed electronics",[15] including printable transistors,[16] solar cells[17] and organic light emitting diodes[18] as emerging field has the potential to meet these goals in future application. However, for these applications a compatible energy source is still lacking. Fully screen printed energy storage devices show great promise for allowing the full integration into manufacturing process of printed electronics.

In flexible and foldable conductors, conducting polymers,[19, 20] graphene,[21, 22] as well as metal nanostructures[23-27] have become dominant research topics. However, conducting polymers and graphene have been demonstrated very limited performance and applications due to the instability, relatively low electrical conductivity or expensive material cost. Metal nanostructures, such as silver nanoparticles and silver nanowires have been printed for flexible electrodes. Chung and co-workers printed silver nanoparticles on wave structured elastomeric substrate with the sheet resistance of 0.44 Ω sq^{-1},[28] Hösel and co-worker printed silver nanoparticles on a thin barrier foil with the sheet resistance of 1.55 Ω sq^{-1},[29] Angmo and co-worker printed silver nanowires on PET with the sheet resistance of 10-20 Ω sq^{-1},[30] etc. The printed silver electrodes showed good flexibility and high conductivity. However, the high cost of silver as a noble and scarce metal has greatly limited its applications in flexible devices. Commercial carbon nanoparticles have obvious advantages for flexible electrodes for their good electrical conductivity, stability and low cost.

CNTs have become attractive nanoscale materials in various applications due to their unique properties. CNTs are promising materials for supercapacitors for their highly accessible surface area, high electrical conductivity and mechanical flexibility as well as high stability.[31, 32] However they seldom direct used in high energy SCs for the low specific capacitance.[33] Transition metal oxides have higher theoretical specific capacitance and better cycling stability compared to carbon materials and conducting polymers, respectively.[34] Since hindered by their poor electrical conductivity pure transition metal oxides always provide low power density.[35] Commonly, CNTs often integrate with other transition metal oxides as electrodes and provide channels for electron transfer in the electrodes.[36] According to the equation: $E = 0.5CV^2$ (C is the specific capacitance, and V is the

cell voltage), symmetric supercapacitors would compromise the specific energy density because of its narrow electrochemical working voltage window. This challenge could be addressed by fabricating ASCs that consist of two different electrodes.[37, 38] i.e. MWCNTs-MnO_2 as the anode and MWCNTs-MoO_3 as the cathode.

In this work, we demonstrate the fabrication of highly conductive electrodes on various flexible substrates by screen printing commercial carbon nanoparticles. Following that MWCNTs-MnO_2 acted as the anode and MWCNTs-MoO_3 acted as the cathode were screen printed on the flexible conductive electrodes. ASCs were made by assembling the above mentioned MWCNTs-MnO_2 anodes and MWCNTs-MoO_3 cathodes. The ASCs show a wide operation potential window of 1.7 V and excellent electrochemical performance, *e.g.* a high energy density of 11.04 mWh cm^{-3} at a power density of 614.6 mW cm^{-3}, a high retained ratio ~91.3% of its initial capacitance after 5000 cycles.

Experimental Details

Carbon nanoparticle, MWCNTs-MnO_2 and MWCNTs-MoO_3 ink production

The carbon nanoparticle ink production was obtained by diluting 2 g commercial carbon ink (CH-8(MOD2)) into 2 ml isophorone, and then glass rod stirring for 2 min. For the MWCNTs-MnO_2 ink production, MnO_2 nanowires (diameters of 8-22 nm, lengths of 0.2-1 μm) were synthesized by a method similar to that reported in the literature.[39] Typically, 9.861 g analytical grade $Mn(CH_3COO)_2{\cdot}4H_2O$ and 9.301 g $(NH_4)_2S_2O_8$ were dissolved by 40 ml distilled water and then hydroalcoholic solution was formed after adding 20 ml 1-octanol. The solution was then transferred into a 100 ml Teflon-lined stainless steel autoclave and solvothermal reaction was performed at 140 ºC for 10 hours. After the reaction, the as-synthesized α-MnO_2 was washed repeatedly by distilled water and high purity ethanol and dried at 60 ºC for 24 h. 200 mg prepared MnO_2 nanowires, 200 mg MWCNTs power (Beijing Boyu Gaoke New Material Technology Co., Ltd) were dissolved by 20 ml ethanol and ultrasonicated for 5 min, then 200 mg ethylcellulose and 1.2g terpineol anhydrous were mixed together in 50 ml sealed beaker by tempestuously agitation at room temperature for 24 h to attain fine dispersion. At last, the solution volatilized to 8 ml. Afterwards, the MWCNTs-MnO_2 ink was obtained. For MWCNTs-MoO_3 ink production, the procedure was similar to the preparation of the MWCNTs-MnO_2 ink. The only difference is that we change the MnO_2 to MoO_3.

Screen printing highly conductive electrodes on various flexible substrates, MWCNTs-MnO_2 anode and MWCNTs-MoO_3 cathode.

In this study, screen printing method is applied. During deposition, the screen is placed a few millimeters above the surface of the substrate. After loading carbon nanoparticle ink onto the screen, a rubber squeegee is swept across the surface of the screen thus bringing the ink into close contact with the substrate. At the same time, the ink flows from the screen to the surface of the substrate. As the screen separates from the substrate, leaving behind ink that dries to yield a desirable electrode. Afterwards, flexible conductive electrodes on clothes, PET, paper were fabricated. For the MWCNTs-MnO_2 anode and MWCNTs-MoO_3 cathode production, the procedure was similar to the preparation of the conductive electrodes.

Assembly of MWCNTs-MnO_2/MWCNTs-MoO_3 ASCs

An ASC with aqueous electrolyte was assembled using a piece of MWCNTs-MnO_2 and a piece of MWCNTs-MoO_3 that they were all printed on PET, with an electrolyte-soaked (4 M LiCl) separator in between. Adhesive tape was used to seal the ASCs.

Characterization

The morphologies, structure, and chemical composition of the flexible conductive electrodes were characterized by high-resolution field emission SEM (FEI Nova Nano-SEM 450), TEM (FEI Titan G2 60-300). The XRD patterns of the samples were recorded with X-ray diffraction (XRD, PANalytical B.V. X'PertPRO). To investigate the flexibility of the electrodes, a three-dimensional (3D) mechanical stage was used to apply a strain on the free end of the sample, with the other end fixed tightly on a manipulation holder. The different slope of the I-V curves which means the resistance of conductive films corresponds to different external compressive strain. Electrochemical measurements including galvanostatic charge/discharge (GCD) curves, cyclic voltammetry (CV) curves, electrochemical impedance spectroscopy (EIS,100 KHz-0.01Hz) were conducted on an electrochemical workstation (CHI 660E). The electrochemical tests of the individual electrode were performed in a three electrode cell, in which carbon electrode and Ag/AgCl electrode was used as the counter and reference electrode, respectively. The electrochemical measurements of the ASC were carried out in a two electrode cell at room temperature in 4 M LiCl electrolyte.

Results and Discussion

The fabrication of highly conductive electrodes, MWCNTs-MnO_2 anode and MWCNTs-MoO_3 cathode is illustrated in Fig. 1a. The rubber squeegee is swept across the surface of the screen thus bringing the carbon nanoparticle, MWCNTs-MnO_2 and MWCNTs-MoO_3 ink into close contact with the substrate. As the squeegee passes over a region, the screen separates from the substrate, leaving behind ink that dries to yield a desirable electrode. The shape of the electrode depends on the pattern of the screen that

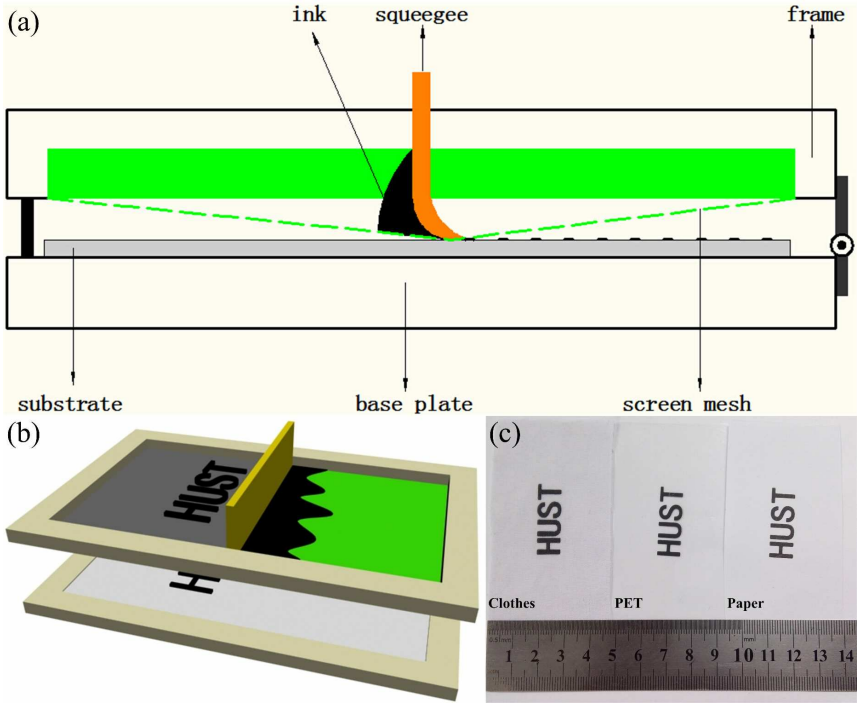

Fig.1 Schematic illustration of the screen-printing process: (a) Cross-sectional illustration of the screen printing method during printing. (b) The pattern on screen for screen printing. (c) A Photo of patterned electrodes on clothes, PET and paper, respectively.

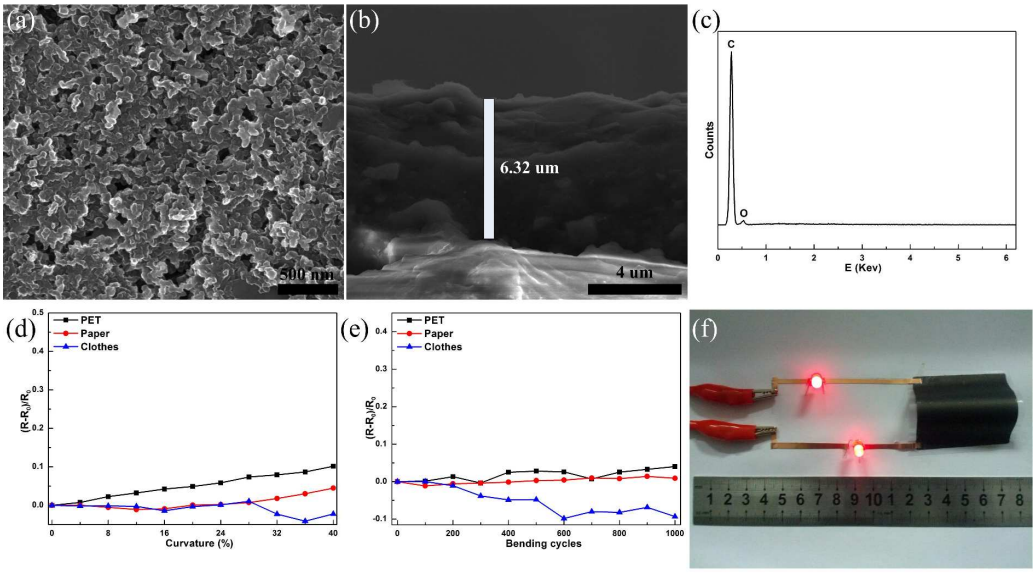

Fig.2 SEM images of (a) surface and (b) side view of screen printed carbon nanoparticle electrode. (c) EDS of carbon nanoparticle electrode. (d) Changes in the electrical resistance of carbon nanoparticle electrode vs. curvature. (e) Changes in the electrical resistance of carbon nanoparticle electrode vs. bending cycles. (f) A foldable circuit by operating a LED on PET with carbon nanoparticle electrode.

was shown in Fig. 1b. Fig.1c shows the photograph of screen printed conductive electrodes on clothes, PET and paper. The microscopic surface morphology of flexible conductive electrode was shown in Fig. 2a. Carbon nanoparticles have a tight connection with each other and form a tangled, dense and homogeneous film. The thickness of the screen printed electrode on PET was 6.32 μm, which can be seen in Fig. 2b. From Fig. 2c we can see the peak of C that came from the carbon nanoparticles and negligible peak of O that came from the binder. In order to further characterize the stability of the electrode, we defined curvature as the bended chord height of total length divided by

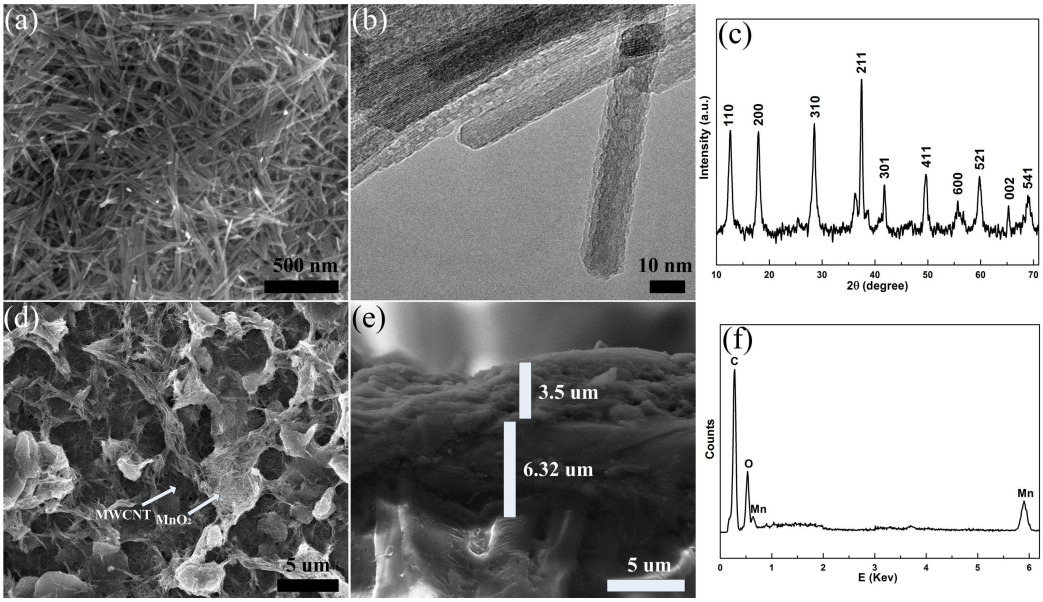

Fig.3 (a) SEM and (b) TEM of the MnO_2 nanowires. (c) XRD patterns of MnO_2 nanowires. SEM images of (d) surface and (e) side view of screen printed MWCNTs-MnO_2 on carbon nanoparticle electrode. (f) EDS of MWCNTs-MnO_2 electrode.

the total length.[40] Fig. 2d and e show the changes in sheet resistance expressed as $(R-R_0)/R_0$, where R_0 is the initial sheet resistance and R is the sheet resistance after bending as a function of curvature. During bending, the changes of the electrodes on clothes, PET and paper did not exceed 4.1%, 10.1% and 4.5%, respectively. After we bend the electrode with a 20% curvature for 1000 times, the changes of sheet resistance on PET were no more than 4%. The compressing process was illustrated in Supporting Fig. S1. A foldable electric circuit was demonstrated by operating a LED on paper with carbon nanoparticle electrode, which was shown in Fig. 2f. The flexible conductive electrode may have potential applications for flexible/foldable optoelectronic devices.

To explore the potential applications in energy storage, we used the carbon nanoparticle electrode as collector on PET, then screen print MWCNTs-MnO_2 and MWCNTs-MoO_3 on it for anode and cathode, respectively. The morphology of MnO_2 nanowires was revealed by SEM and TEM images (Fig. 3a and b). MnO_2 nanowires entangled with each other with a length of 0.2-1 μm and diameters of 8-22 nm. (Supporting Fig. S2 a)

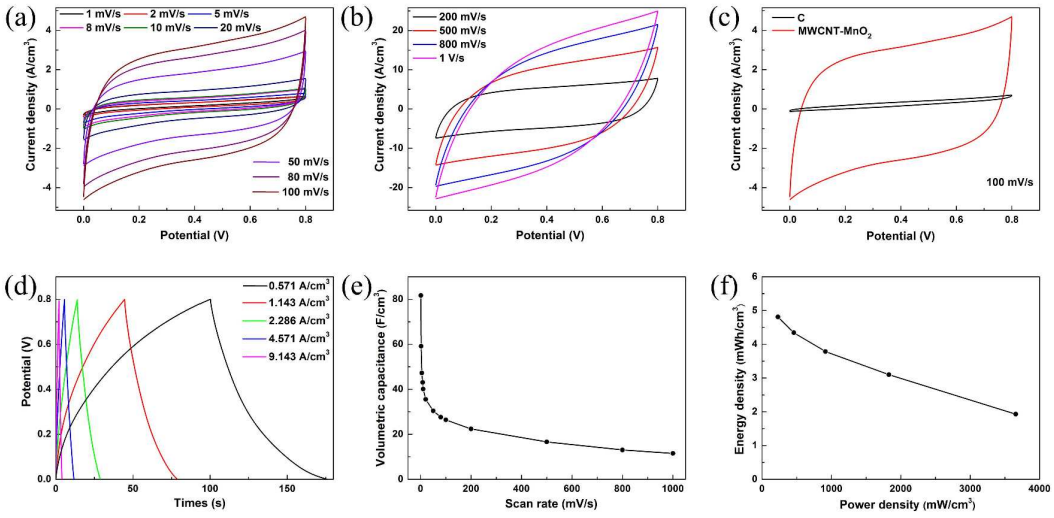

Fig. 4 Electrochemical performance of the MWCNTs-MnO_2 electrodes. Cyclic voltammograms of the MWCNTs-MnO_2 electrodes with scan rate (a) from 0.001 V s^{-1} to 0.1 V s^{-1} and (b) from 0.2 V s^{-1} to 1 V s^{-1}. (c) Cyclic voltammograms of the carbon nanoparticle and MWCNTs-MnO_2 electrodes at the scan rate of 0.1 Vs^{-1} (d) Galvanostatic charge discharge behavior of MWCNTs-MnO_2 electrodes. (e) Volumetric capacitance *vs* scan rate. (f) Energy and power density plot.

The X-ray diffraction (XRD) pattern (Fig. 3c) confirmed that the crystal type of the nanowire belongs to the tetragonal α-MnO_2 phase (JCPDS 44-0141). Fig. 3d is a SEM of MWCNTs-MnO_2 composites, revealing that there are few conglobations of CNTs, which ensures that the conductive channels are uniformly distributed throughout the whole electrode. The thickness of the MWCNTs-MnO_2 electrode was 3.5 μm that can be seen in Fig. 3e. The enlarger SEM image of the border of carbon nanoparticle and MWCNTs-MnO_2 was shown in Supporting Fig. S2 b. The peaks of C, O and Mn that can be seen in Fig. 3f further confirm the ingredients. The MWCNTs and MnO_2 ink were also printed on PET and the microscopic surface morphology of the electrodes could be seen in Supporting Fig. S2 c and d. CV and GCD curves are generally used to characterize the capacitive behavior of an electrode material. Fig. 4a and b present curves of the anodes with the scanning rates from 1 mV s^{-1} to 1 V s^{-1}. As expected, the electrode showed ideal capacitive behavior with rectangular CV curves. The MWCNTs-MnO_2 electrode exhibited substantially larger current density than carbon nanoparticle electrode (Fig. 4c) because MnO_2 is more electrochemically active than carbon nanoparticle. For comparison we also test the CV curves of MWCNTs electrodes and MnO_2 electrodes. As shown in Supporting Fig. S3, the MWCNTs-MnO_2 electrode also exhibited substantially larger current density than both MWCNTs electrodes and MnO_2 electrodes for good conductivity and activity of the MWCNTs-MnO_2 composite. GCD measurements were carried out to further evaluate the electrochemical performances of the MWCNTs-MnO_2 anode. Fig. 4d shows the GCD curves of the MWCNTs-MnO_2 electrode at different current densities, in which good linear potential–time profiles are achieved, demonstrating a good capacitance performance of the electrode. The volumetric capacitance that decreased with the scanning rate (see Figure 4e) was evaluated by the above CV results. At the scan rate of 1 mV s^{-1}, the volumetric capacitance of the anode was 81.7 F cm^{-3}. Fig. 4f shows the Ragone plot for the energy density and the power density of the anode, high energy density of 4.81 mWh cm^{-3} at a power density of 228.4 mW cm^{-3}. Moreover, a high power density of 3.66 W cm^{-3} was obtained, and the energy density was still as high as 1.93 mWh cm^{-3} at a discharge current density of 9.143 A cm^{-3}.

It is well known that charge balance between positive and negative electrodes is crucial to maximize the energy density of ASCs.[41] So MWCNTs-MoO_3 negative electrodes were screen printed with different ratio. For better screen printing MoO_3 on PET without clogging the screen, we ball-milling the MoO_3. Supporting Fig. S4 a and b shows the SEM images of MoO_3 before and after ball-milling, respectively. From Supporting Fig. S4 c, we can see the peaks of Mo and O that came from MoO_3 and the peak of C came from conducting resin. MoO_3 nanoparticles are distributed around the MWCNTs and have a tight connection with MWCNTs and the thickness of MWCNTs-MoO_3 negative electrode was 4.8 μm (Supporting Fig. S4 d and e). Supporting Fig. S4 f further confirms the ingredients of the negative electrode. The MoO_3 ink was also printed and the microscopic surface morphology of the electrodes could be seen in Supporting Fig. S5.

CV and GCD curves are also generally used to characterize the capacitive behavior of the negative electrode. The capacitance of MWCNTs-MoO_3 negative electrode with the ratio of 1:1.5 was the most

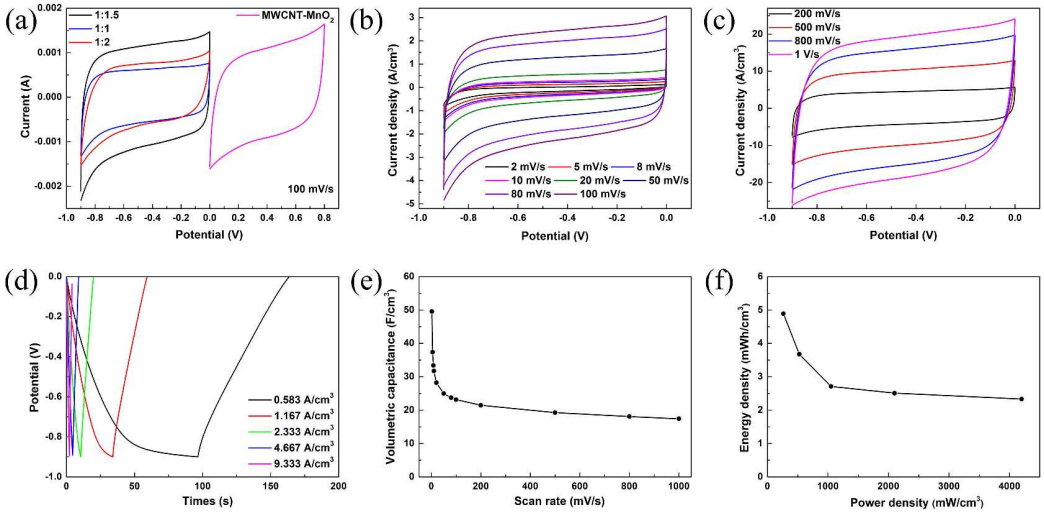

Fig. 5 Electrochemical performance of the MWCNTs-MoO_3 electrodes. (a) CV curves of the cathodes with different ratio and of the MWCNTs-MnO_2 anode (the scan rate of 0.1 V s^{-1}). Cyclic voltammograms of the MWCNTs-MoO_3 electrodes with scan rate (b) from 0.002 V s^{-1} to 0.1 V s^{-1} and (c) from 0.2 V s^{-1} to 1 V s^{-1}. (d) Galvanostatic charge discharge behavior of MWCNTs-MoO_3 electrodes. (e) Volumetric capacitance *vs* scan rate. (f) Energy and power density plot.

closed to positive electrodes at the scanning rate of 100 mV s^{-1} (Fig. 5a). Fig. 5b and c present curves of the cathodes with the scanning rates from 2 mV s^{-1} to 1 V s^{-1}. As expected, the electrode showed ideal capacitive behavior with rectangular CV curves. We also test the CV curves of MWCNTs electrodes and MoO_3 electrodes. As shown in Supporting Fig. S6, the MWCNTs-MoO_3 electrode also exhibited substantially larger current density than both MWCNTs electrodes and MoO_3 electrodes. Good linear potential–time profiles are achieved in GCD curves of the MWCNTs-MoO_3 electrode at different current densities, demonstrating a good capacitance performance of the negative electrode (Fig. 5d). The cathode obtained a volumetric capacitance of 49.5 F cm^{-3} at the scanning rate of 2 mV s^{-1} and a high energy density of 4.89 mWh cm^{-3} at a power density of 262.3 mW cm^{-3} (Fig. 5e and f).

To further investigate the performances of the asymmetric supercapacitor fabricated with screen-printed MWCNTs-MnO_2 anode (mass density of 0.4 mg cm^{-2}) and well matched MWCNTs-MoO_3 cathode (mass density of 0.6 mg cm^{-2}), a variety of electrochemical measurements have performed using two electrode configurations. The CV measurements indicated that the device exhibited a stable potential window up to 1.7 V (Fig. 6a). The large potential window means a high energy density, which is a

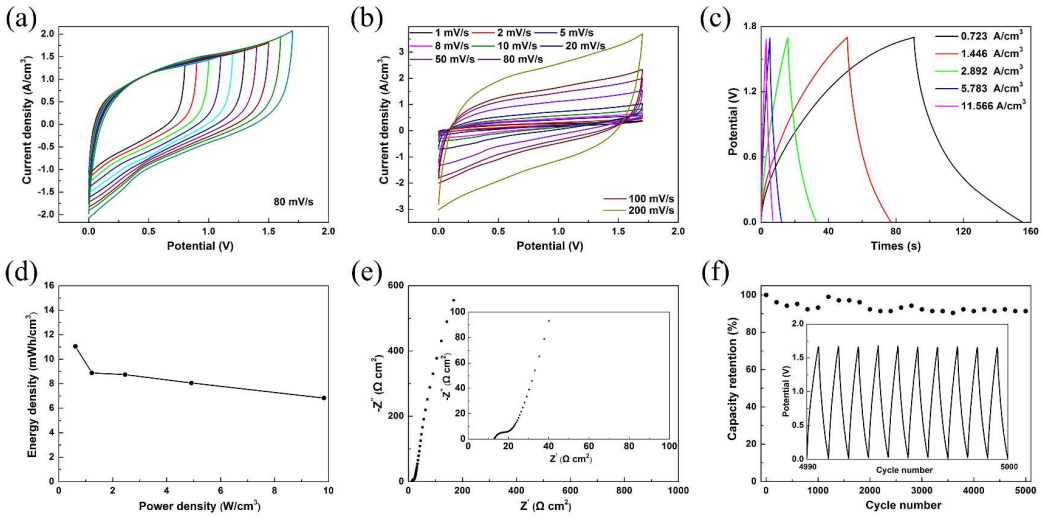

Fig. 6 Electrochemical performances of the ASC. (a) CV curves of the device at different potential windows, the scan rate is 80 mV s^{-1}. (b) CV curves of the device at different scan rate. (c) Galvanostatic discharge curves of the device at different current density. (d) Energy and power density plot. (e) Nyquist plot. (f) Cycle life, inset shows the GCD curve from 4990th to 5000th.

major advantage compared to common symmetric supercapacitor and a very important factor to meet the demand of application. As shown in Fig. 6b, the asymmetric supercapacitor had well symmetrical and near rectangular CV curves at the potential window of 0-1.7 V, indicating that the device also had good capacitance performance. Good linear profiles of GCD curves with different current densities (Fig. 6c) further confirm the perfect electrochemical behaviour of the device. The asymmetric supercapacitor showed high energy of 11.04 mWh cm^{-3} at a power density of 614.6 mW cm^{-3}. Moreover, a high power density of 9.8 W cm^{-3} was obtained, and the energy density was still as high as 6.83 mWh cm^{-3} at a discharge current density of 11.566 A cm^{-3}. (Fig. 6d) It is notable that the highest E and P of this ASC are much higher than those in the previous reports.[42, 43] Fig. 6e presented the impedance spectrum of the as-fabricated device which exhibited a negligible 45° Warburg region and the ESR value (13 Ω) of the device, indicating the fast ion transport at the active material-electrolyte interface. The impedance spectrum becomes almost a vertical line where the imaginary part of impedance increases dramatically in low frequency range, showing the perfect capacitive behaviour of ion diffusion in the electrode materials. The long-term cycle stability was measured by GCD at a current density of 1.928 A cm^{-3} for 5000 cycles and the result is shown in Fig. 6f. The capacitance only had a slight fuctuation in the whole process. The capacity retention is 91.3% after 5000 cycles, which is higher than the previous reports.[44, 45] This implied the good charge-discharge reversibility of the device.

Conclusions

Highly flexible conductive electrodes have been successfully prepared by screen printing carbon nanoparticle ink onto various substrates. The flexible electrodes showed good stability during the bending test and could act as a foldable electric circuit. An asymmetric supercapacitor was fabricated by assembling a screen printed MWCNTs-MnO_2 anode and MWCNTs-MoO_3 cathode. The supercapacitor has a wide operating potential window of 1.7 V and exhibits excellent electrochemical performance, *e.g.* a

high density of 11.04 mWh cm^{-3} at a power density of 614.6 mW cm^{-3}, a high retained ratio ~91.3% of its initial capacitance after 5000 cycles. The screen-printing acting as a versatile, simple, fast, cost-effective printing techniques method can be fully integrated with the fabrication process in current printed electronics and has potential applications for energy storage.

Acknowledgements

This work was supported by the National Natural Science Foundation of china (11204093, 11374110), Overseas Master Program (MS2011HZKJ043), and the Fundamental Research Funds for the Central Universities (HUST: 2014TS124). Y.H.G would like to thank Prof. Zhong-Lin Wang for the support of experimental facilities in WNLO of HUST.

Notes and references

[a]*Center for Nanoscale Characterization & Devices (CNCD), Wuhan National Laboratory for Optoelectronics (WNLO) & School of Physics, Huazhong University of Science and Technology (HUST), LuoyuRoad 1037, Wuhan 430074, China. E-mail:gaoyihua@hust.edu.cn; nishuang_liu@foxmail.com*

[b]*Hubei Collaborative Innovation Center for Advanced Organic Chemical Materials, Hubei University, 368 Youyi Avenue, Wuhan 430062, China*

1. L. S. Zhou, A. Wanga, S. C. Wu, J. Sun, S. Park and T. N. Jackson, *Appl. Phys. Lett.*, 2006, **88**, 3.
2. Y. Chen, J. Au, P. Kazlas, A. Ritenour, H. Gates and M. McCreary, *Nature*, 2003, **423**, 136-136.
3. B. D. Braaten, S. Roy, S. Nariyal, M. Al Aziz, N. F. Chamberlain, I. Irfanullah, M. T. Reich and D. E. Anagnostou, *Ieee T. Antenn. Propag.*, 2013, **61**, 655-665.
4. A. Rida, L. Yang, R. Vyas and M. M. Tentzeris, *Ieee Antenn. Propag. M.*, 2009, **51**, 13-23.
5. L. Huang, Y. Huang, J. Liang, X. Wan and Y. Chen, *Nano Res.*, 2011, **4**, 675-684.
6. V. Marin, E. Holder, M. M. Wienk, E. Tekin, D. Kozodaev and U. S. Schubert, *Macromol. Rapid Comm.*, 2005, **26**, 319-324.
7. L. Catarinucci, S. Tedesco and L. Tarricone, *Ieee Sens. J.*, 2013, **13**, 783-791.
8. H. Hu, K. Zhang, S. Li, S. Jia and C. Ye, *J. Mater. Chem. A*, 2014, **2**, 20916-20922.
9. L. Fan, N. Zhang and K. Sun, *Chem. Commun.*, 2014, **50**, 6789-6792.
10. D. Pech, M. Brunet, P.-L. Taberna, P. Simon, N. Fabre, F. Mesnilgrente, V. Conedera and H. Durou, *J. Power Sources*, 2010, **195**, 1266-1269.
11. C. Guillen and J. Herrero, *Opt. Commun.*, 2009, **282**, 574-578.
12. C. Wang, C. Wang and Y. Mao, *Acta Photonica Sinica*, 2013, **42**, 812-816.
13. L. G. De Arco, Y. Zhang, C. W. Schlenker, K. Ryu, M. E. Thompson and C. W. Zhou, *ACS Nano*, 2010, **4**, 2865-2873.
14. X. Xiao, X. Peng, H. Jin, T. Li, C. Zhang, B. Gao, B. Hu, K. Huo and J. Zhou, *Adv. Mater.*, 2013, **25**, 5091-5097.
15. M. Berggren, D. Nilsson and N. D. Robinson, *Nat. Mater.*, 2007, **6**, 3-5.
16. H. Yan, Z. H. Chen, Y. Zheng, C. Newman, J. R. Quinn, F. Dotz, M. Kastler and A. Facchetti, *Nature*, 2009, **457**, 679-686.
17. F. C. Krebs, *Sol. Energ. Mat. Sol. C.*, 2009, **93**, 394-412.
18. D. A. Pardo, G. E. Jabbour and N. Peyghambarian, *Adv. Mater.*, 2000, **12**, 1249-1252.
19. D. S. Hecht, L. Hu and G. Irvin, *Adv. Mater.*, 2011, **23**, 1482-1513.
20. A. A. Argun, A. Cirpan and J. R. Reynolds, *Adv. Mater.*, 2003, **15**, 1338-1341.
21. G. Eda, G. Fanchini and M. Chhowalla, *Nat. Nanotechnol.*, 2008, **3**, 270-274.
22. K. S. Kim, Y. Zhao, H. Jang, S. Y. Lee, J. M. Kim, K. S. Kim, J.-H. Ahn, P. Kim, J.-Y. Choi and B. H. Hong, *Nature*, 2009, **457**, 706-710.
23. D. C. Hyun, M. Park, C. Park, B. Kim, Y. Xia, J. H. Hur, J. M. Kim, J. J. Park and U. Jeong, *Adv. Mater.*, 2011, **23**, 2946-2950.
24. L. Hu, H. S. Kim, J.-Y. Lee, P. Peumans and Y. Cui, *ACS Nano*, 2010, **4**, 2955-2963.
25. I. E. Stewart, A. R. Rathmell, L. Yan, S. Ye, P. F. Flowers, W. You and B. J. Wiley, *Nanoscale*, 2014, **6**, 5980-5988.
26. F. Guo, H. Azimi, Y. Hou, T. Przybilla, M. Hu, C. Bronnbauer, S. Langner, E. Spiecker, K. Forberich and C. J. Brabec, *Nanoscale*, 2015, **7**, 1642-1649.
27. Y. Zhao, Y. Zhang, Y. Li, Z. He and Z. Yan, *RSC Adv.*, 2012, **2**, 11544-11551.
28. S. Chung, J. Lee, H. Song, S. Kim, J. Jeong and Y. Hong, *Appl. Phys. Lett.*, 2011, **98**.
29. M. Hosel and F. C. Krebs, *J. Mater. Chem.*, 2012, **22**, 15683-15688.
30. D. Angmo, T. R. Andersen, J. J. Bentzen, M. Helgesen, R. R. Sondergaard, M. Jorgensen, J. E. Carle, E. Bundgaard and F. C. Krebs, *Adv. Funct. Mater.*, 2015, **25**, 4539-4547.
31. J. Y. Tao, N. S. Liu, J. Y. Rao, L. W. Ding, M. R. Al Bahrani, L. Y. Li, J. Su and Y. H. Gao, *Nanoscale*, 2014, **6**, 15073-15079.
32. M. F. L. De Volder, S. H. Tawfick, R. H. Baughman and A. J. Hart, *Science*, 2013, **339**, 535-539.
33. E. Frackowiak and F. Beguin, *Carbon*, 2001, **39**, 937-950.
34. H. Jiang, J. Ma and C. Z. Li, *Adv. Mater.*, 2012, **24**, 4197-4202.
35. N. S. Liu, W. Z. Ma, J. Y. Tao, X. H. Zhang, J. Su, L. Y. Li, C. X. Yang, Y. H. Gao, D. Golberg and Y. Bando, *Adv. Mater.*, 2013, **25**, 4925-4931.
36. Y. Jin, H. Y. Chen, M. H. Chen, N. Liu and Q. W. Li, *ACS Appl. Mater. Inter.*, 2013, **5**, 3408-3416.
37. J. Y. Tao, N. S. Liu, L. Y. Li and Y. H. Gao, *Nanoscale*, 2014, **6**, 2922-2928.
38. C. X. Yang, Y. L. Shi, N. S. Liu, J. Y. Tao, S. L. Wang, W. J. Liu, Y. M. Wang, J. Su, L. Y. Li, C. P. Yang and Y. H. Gao, *RSC Adv.*, 2015, **5**, 45129-45135.
39. H. W. Lee, P. Muralidharan, R. Ruffo, C. M. Mari, Y. Cui and D. K. Kim, *Nano Lett.*, 2010, **10**, 3852-3856.
40. S. Wang, N. Liu, J. Tao, C. Yang, W. Liu, Y. Shi, Y. Wang, J. Su, L. Li and Y. Gao, *J. Mater. Chem. A*, 2015, **3**, 2407-2413.
41. J. P. Zheng, *J. Electrochem. Soc.*, 2003, **150**, A484-A492.
42. Z. Weng, Y. Su, D.-W. Wang, F. Li, J. Du and H.-M. Cheng, *Adv. Energy Mater.*, 2011, **1**, 917-922.
43. Y. B. Xie and X. Q. Fang, *Electrochim. Acta*, 2014, **120**, 273-283.
44. F. Yang, M. Zhao, Q. Sun and Y. Qiao, *RSC Adv.*, 2015, **5**, 9843-9847.
45. Y. Gao, Y. S. Zhou, M. Qian, H. M. Li, J. Redepenning, L. S. Fan, X. N. He, W. Xiong, X. Huang, M. Majhouri-Samani, L. Jiang and Y. F. Lu, *RSC Adv.*, 2013, **3**, 20613-20618.

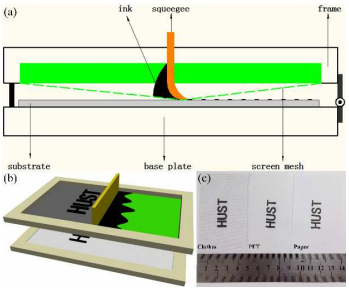

Screen printing of MWCNTs-MnO_2 anodes and MWCNTs-MoO_3 cathodes on carbon nanoparticle flexible electrodes for supercapacitors.